Evidence for a spontaneous gapped state in ultraclean bilayer graphene

Wenzhong Bao[a,b,1], Jairo Velasco, Jr.[a,1], Fan Zhang[c,d,1], Lei Jing[a], Brian Standley[e], Dmitry Smirnov[f], Marc Bockrath[a], Allan H. MacDonald[c,2], and Chun Ning Lau[a,2]

[a]Department of Physics and Astronomy, University of California, 900 University Avenue, Riverside, CA 92521; [b]Department of Physics, University of Maryland, College Park, MD 20742; [c]Department of Physics, University of Texas at Austin, Austin, TX 78712; [d]Department of Physics and Astronomy, University of Pennsylvania, Philadelphia, PA 19104; [e]Department of Applied Physics, California Institute of Technology, Pasadena, CA 90211; and [f]National High Magnetic Field Laboratory, Tallahassee, FL 32310

Contributed by Allan H. MacDonald, April 19, 2012 (sent for review February 1, 2012)

At the charge neutrality point, bilayer graphene (BLG) is strongly susceptible to electronic interactions and is expected to undergo a phase transition to a state with spontaneously broken symmetries. By systematically investigating a large number of single-and double-gated BLG devices, we observe a bimodal distribution of minimum conductivities at the charge neutrality point. Although $\sigma_{\min}$ is often approximately 2–3 e^2/h (where e is the electron charge and h is Planck's constant), it is several orders of magnitude smaller in BLG devices that have both high mobility and low extrinsic doping. The insulating state in the latter samples appears below a transition temperature T_c of approximately 5 K and has a $T = 0$ energy gap of approximately 3 meV. Transitions between these different states can be tuned by adjusting disorder or carrier density.

topological states | anomalous hall | spontaneous quantum Hall states | electron–electron interactions | layer antiferromagnets

Bilayer graphene (BLG) has provided a fascinating new platform for both post-silicon electronics and exotic many-body physics (1–23). Because its conduction and valence bands touch at two points in momentum space and have approximately quadratic dispersion accompanied by momentum-space pseudospin textures with vorticity $J = 2$, charge-neutral BLG is likely to have a broken-symmetry ground state in the absence of disorder (6–11, 15–18, 24–26). Theoretical work on the character of the ground state in neutral BLG has examined a variety of distinct but related pseudospin ferromagnet states—including gapped anomalous Hall (5, 6, 19), layer antiferromagnetic (6–8, 16–18, 22), and current loop states (26)—that break time-reversal symmetry, and gapless nematic states, which alter Dirac point structure and reduce rotational symmetry (6–11, 15–18, 24, 25). The pseudospin degree of freedom reflects the presence of two low-energy carbon sites per unit cell that are localized in different layers. Experimental work has confirmed the strong role of interactions, but has been equivocal in specifying ground-state properties. In particular, both gapped and gapless states have been reported (19–23) in suspended BLG. The low-temperature minimum conductivity at the charge neutrality point (CNP), $\sigma_{\min}$, has ranged from approximately 0.05 to 250 μS. These orders-of-magnitude differences between $\sigma_{\min}$ values measured in apparently similar samples have been baffling.

In this paper we attempt to shed light on these ambiguous findings by systematically examining a large number of single-and double-gated BLG samples, with mobility values ranging from 500 to 2,000 $\mathrm{cm^2/V{\cdot}s}$ for substrate-supported samples and 6,000 to 350,000 for suspended samples. We find a surprisingly constant $\sigma_{\min}$ value of approximately 2–3 e^2/h for a majority of the devices (here, e is the electron charge and h is Planck's constant), independent of their mobility and of the presence or absence of substrates. However, for T below approximately 5 K, the best devices form an insulating state with an energy gap of approximately 2–3 meV. Importantly, the transition between conducting and insulating states can also be tuned by varying charge density n and perpendicular electric field $E_\perp$, in agreement with theoretical predictions for gapped pseudospin ferromagnetic states. Finally, our observation of a bimodal distribution of $\sigma_{\min}$ values suggests that transport in the conducting devices could occur along domain boundaries that separate regions with different pseudospin order configurations.

Results

We fabricate single-gated BLG devices using a lithography-free technique and suspend double-gated BLG by combining acid etching with a multilevel lithographic technique to make devices with suspended top gates (*SI Text*). All suspended BLG devices as fabricated have relatively low mobilities, presumably due to gas or water absorption on the surface of BLG exposed to an ambient environment. Current annealing is performed in vacuum (Fig. 1*C*). The optimal state is normally achieved when I starts to saturate (*SI Text*) at approximately 0.2 mA/μm per layer.

Fig. 1 *D* and *E* plot the two-terminal differential conductivity $\sigma = (L/W)dI/dV$ of two suspended BLG devices vs. back-gate voltage V_{bg} at $T = 1.5$ K after current annealing. (Here, L/W is the aspect ratio of the devices.) Both curves are steeply V shaped and have CNPs (marked by conductivity minima) that are close to $V_{bg} = 0$ V. Surprisingly, the $\sigma_{\min}$ values of the two devices are drastically different: 2.5 and 0.02 e^2/h, respectively. The insulating behavior of the latter device is confirmed by current–voltage I-V_{sd} curves. In a magnetic field B, both devices display quantum Hall plateaus with the eightfold degeneracy (12, 13) of the zero-energy Landau level (LL) fully lifted (*SI Text*). From the Landau fan diagram that plots the differential conductance G (color) vs. V_{bg} and B (Fig. 1 *D* and *E*, *Insets*), the $\nu = 0$ state is visible for both devices at $B > 0.5$ T and persists down to $B = 0$ for the device with very low $\sigma_{\min}$ (21, 22).

To shed light on the origin of the large range of $\sigma_{\min}$ values, we investigated nine substrate-supported BLG devices and 23 suspended BLG devices with aspect ratios between 0.5 and 2, and areas from 1 to 18 μm^2. The results are summarized in Fig. 2*A*, which plots $\sigma_{\min}$ as a function of field-effect mobility $\mu = \frac{1}{e}\frac{d\sigma}{dn}$ for each device. Evidently, the data points separate into two groups. Most data points fall into group I, in which $\sigma_{\min}$ is almost independent of mobility and similar for suspended and supported devices. Within this class of devices, the CNP conductivity is approximately 100 μS or approximately 2.8 e^2/h (27–33).

Author contributions: W.B., J.V.J., M.B., and C.N.L. designed research; W.B., J.V.J., L.J., B.S., D.S., and C.N.L. performed research; W.B., J.V.J., F.Z., M.B., A.H.M., and C.N.L. analyzed data; and W.B., J.V.J., F.Z., M.B., A.H.M., and C.N.L. wrote the paper.

The authors declare no conflict of interest.

[1]W.B., J.V., and F.Z. contributed equally to this work.

[2]To whom correspondence may be addressed. E-mail: macd@physics.utexas.edu or jeaniel@ucr.edu.

This article contains supporting information online at www.pnas.org/lookup/suppl/doi:10.1073/pnas.1205978109/-/DCSupplemental.

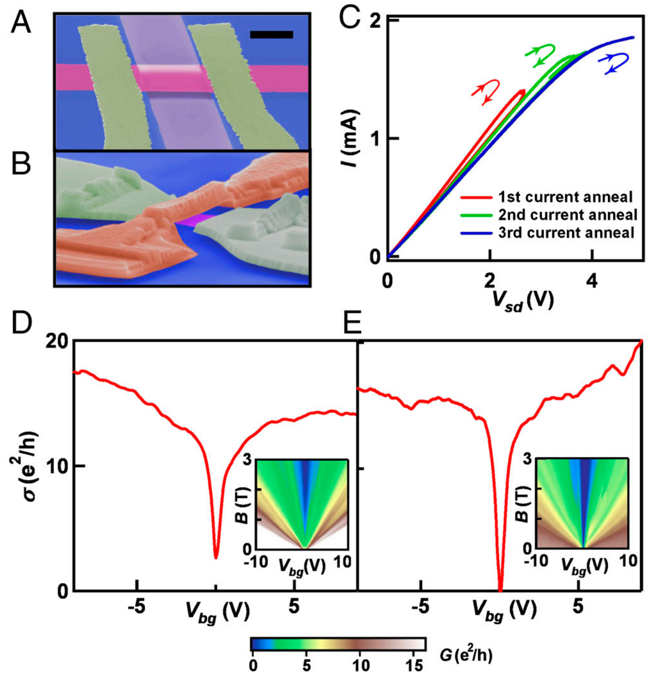

Fig. 1. (*A*, *B*) False color-scanning electron micrograph of BLG device with and without top gate (Scale bar: 2 μm). (*C*) *I*-V_{sd} curves of a suspended BLG during current annealing. (*D*, *E*: *Main* and *Insets*) $\sigma(V_g)$ and $G(V_{\mathrm{bg}}, B)$ for two BLG devices with and without insulating state at CNP ($T = 1.5$ K).

Very different behavior is found in the seven devices that fall into group II: $\sigma_{\min}$ is at most 0.4 e^2/h, and as low as 1 μS. Notably, all seven devices have very high mobility. To identify the physical difference between the two classes of devices, we also examined V_{CNP} (the V_{bg} required to reach the CNP, which is a proxy for the overall doping level). Fig. 2 *B* and *C* plots $\sigma_{\min}$ and μ vs. V_{CNP} for all suspended samples, with the insulating devices denoted by blue triangles. Two striking features are evident: (*i*) μ decreases with increasing V_{CNP} in agreement with previous reports in substrate-supported graphene (34, 35), suggesting that charged impurities are important scatterers even in these high-mobility devices; and (*ii*) the insulating BLG devices in Fig. 2 *B* and *C* cluster around $V_{\mathrm{CNP}} = 0$. Insulating behavior at the CNP is observed only in devices with *both* high mobility and low charged-impurity density.

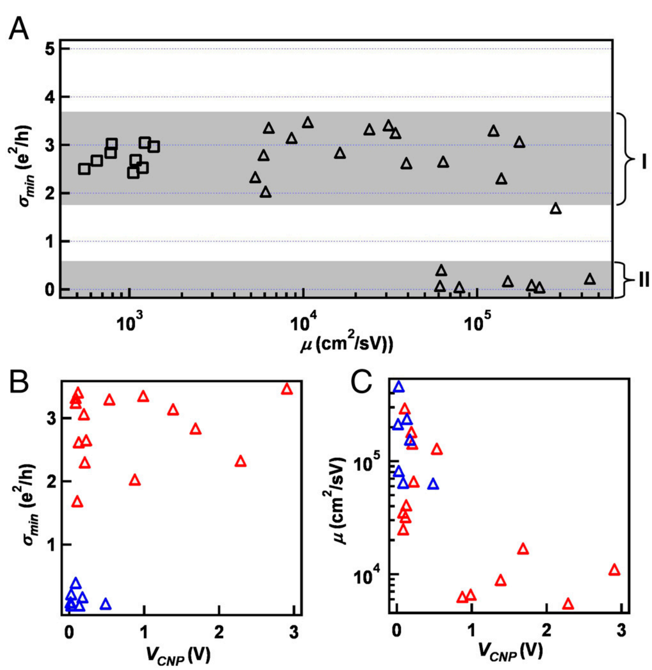

Fig. 2. (*A*) $\sigma_{\min}(\mu)$ for ninesubstrate-supported BLG devices (square symbols) and 23 suspended BLG devices (triangular symbols) at 1.5 K (except for three devices in region II, which was taken at $T = 0.3$ K). (*B*, *C*) $\mu(V_{\mathrm{CNP}})$ and $\sigma_{\min}(V_{\mathrm{CNP}})$ for suspended BLG devices. The blue symbols denote devices in region II.

To obtain further insight we compare the temperature dependences of group I and group II devices. Fig. 3*A* displays $\sigma_{\min}$ on a logarithmic scale vs. $1/T$ for $1.4 \le T \le 100$ K for one non-insulating device and two different insulating BLG devices. The inset plots the same data sets $\sigma_{\min}(T)$ on linear-log scales. Amazingly, for $10 < T < 100$ K, the $\sigma_{\min}(T)$ curves of all three devices collapse into a single curve. This is in contrast with previous work on single-layer (36) and trilayer graphene (37, 38), which reported large sample-to-sample variation in $\sigma_{\min}(T)$. The consistent behaviors among three devices for $T > 10$ K strongly suggest that we are indeed observing intrinsic attributes of BLG.

The behaviors of the device classes start to deviate at approximately 5–7 K: $\sigma_{\min}$ of the non-insulating device decreases only modestly; in contrast, the $\sigma_{\min}$ of both insulating devices exhibits an abrupt change in slope and drops precipitously for $T < 5$ K where the data are well described by $\sigma_{\min}(T) = A\exp(-E_A/2\,k_B T)$. (Here, A is the prefactor, E_A is the activation energy, and k_B is the Boltzmann's constant). The best fit is obtained by using $A = 17\ e^2/h$ and E_A/k_B of approximately 18 K, indicating thermally activated transport over a gap $E_A = 1.6$ meV.

These data suggest the presence of a gap in insulating devices for $T < 5$ K. To investigate this further, we study σ vs. source-drain bias V_{sd} at the CNP (21, 22) (Fig. 3*B*). At $T = 1.4$ K, σ increases precipitously when $|V_{\mathrm{sd}}|$ increases from 0, forming a U-shaped profile and reaching two dramatic peaks at ± 2.8 mV, and decreases again to approximately 8 e^2/h for $|V_{\mathrm{sd}}| > 5$ mV. These $\sigma(V_{\mathrm{sd}})$ curves resemble the density of states of gapped phases, like superconductors, charge density waves, and, perhaps most pertinently, the displacement field-induced gapped BLG state (4, 39–41). Because the device has symmetric coupling to both electrodes, we take the magnitude of the gap to be half of the separation between the two peaks (approximately 2.8 meV). This is larger than the value of approximately 1.6 meV obtained from thermal-activation measurements, possibly reflecting the contribution of variable range hopping and other disorder-related effects to the temperature dependence of transport. Thus, the $\sigma(V_{\mathrm{sd}})$ curves, together with the $\sigma_{\min}(T)$ measurements, unequivocally establishes the presence of a low-temperature gap of approximately 2–3 meV in the charged excitation spectrum of insulating devices.

We now examine the $\sigma(V_{\mathrm{sd}})$ curves of the insulating devices at different temperatures (Fig. 3*B*). When T increases from 1.4 K, $\sigma_{\min}$ increases, $\sigma(V_{\mathrm{sd}})$ adopts a V-shaped profile, and the magnitudes of the two peaks decrease and vanish entirely at approximately 5 K. These observations suggest the disappearance of the gap for $T > 5$ K. Our data thus provide strong evidence for a finite temperature phase transition to a gapped state with a critical temperature T_c of approximately 5 K and a gap Δ/k_B (approximately 20–30 K). The temperature dependence of the gap strongly suggests that it is of many-body origin, and the rough correspondence between the critical temperature and gap scales suggests that the broken symmetry is reasonably well described by mean-field theory (*SI Text*).

Our data thus far suggest a T-dependent phase transition in charge-neutral BLG between a conducting state and an interaction-induced insulating state. The conducting state could be due to bulk two-dimensional metallic behavior, or, alternatively, due to transport along topologically protected edge states supported by domain walls separating regions (5, 6) with different spin-and valley-dependent Chern numbers. Future experiments will be

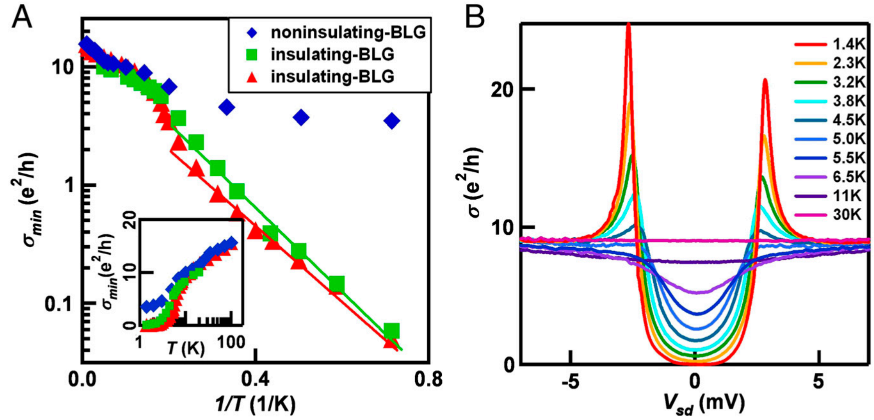

Fig. 3. (*A*) $\sigma_{\min}(1/T)$ for insulating and non-insulating BLG devices. (*Inset*)$\sigma_{\min}(T)$ of data set. The solid lines are fits to data $T < 5$ K to Eq. **1**. (*B*) T-dependence of $\sigma(V_{\rm sd})$ at CNP for an insulating BLG device.

necessary to ascertain the nature of the conducting electronic state at the CNP.

An intriguing possibility is that a quantum phase transition (i.e., one that is tuned by parameters other than T, such as disorder, carrier density, or electric field) may take place at $T = 0$. To this end, we examine the $\sigma(V_{\rm sd})$ curves of two conducting devices that have mobility 140,000 and 24,000 $\mathrm{cm}^2/(\mathrm{Vs})$, respectively, at $T = 1.4$ K (Fig. 4*A*). Data from an insulating device are also plotted for comparison. Remarkably, at higher temperatures the $\sigma(V_{\rm sd})$ curves of both conducting devices bear a striking resemblance to those of insulating BLG. In particular, the device with $\mu = 140{,}000$ $\mathrm{cm}^2/(\mathrm{Vs})$ has a V-shaped profile at small $V_{\rm sd}$, elevated $\sigma_{\min}$ and smaller peaks at $V_{\rm sd}$ of approximately ± 2.5 mV, and resembles the curve in Fig. 3*B* at T of approximately 4 K. For the device with $\mu = 24{,}000$ $\mathrm{cm}^2/(\mathrm{Vs})$, $\sigma(V)$ is flatter and without the side peaks, thus resembling the curve from the insulating device at T of approximately 10 K. Taken together, charge disorder and temperature have similar effects on the insulating state in BLG.

Finally, we examine the effect of carrier density n and an applied $E_\perp$ that induces an interlayer potential difference (*SI Text*) In our double-gated BLG devices we can control n and $E_\perp$ independently. Several line traces of $\sigma(V_{\rm sd})$ at $n = 0$ for different values of $E_\perp$ are shown in Fig. 4*B*. As $E_\perp$ decreases from 0 to −7 mV/nm, the U-shaped $\sigma(V_{\rm sd})$ curve becomes V shaped, with less prominent side features and an elevated $\sigma_{\min}$ (i.e., the gap size appears to be diminished by $E_\perp$). For still larger fields, the well-known single-particle gap of unbalanced bilayers gradually emerges (2, 4, 41). On the other hand, the influence of total carrier density on the insulating state is extremely sharp. At $E_\perp = 0$ (Fig. 4*C*), a small density n of approximately 6.2×10^9 cm^{-2} is sufficient to obscure significantly the gapped correlated state; when n is approximately 1.2×10^{10} cm^{-2}, the gapped feature completely vanishes and $\sigma_{\min}$ reaches approximately 5 e^2/h.

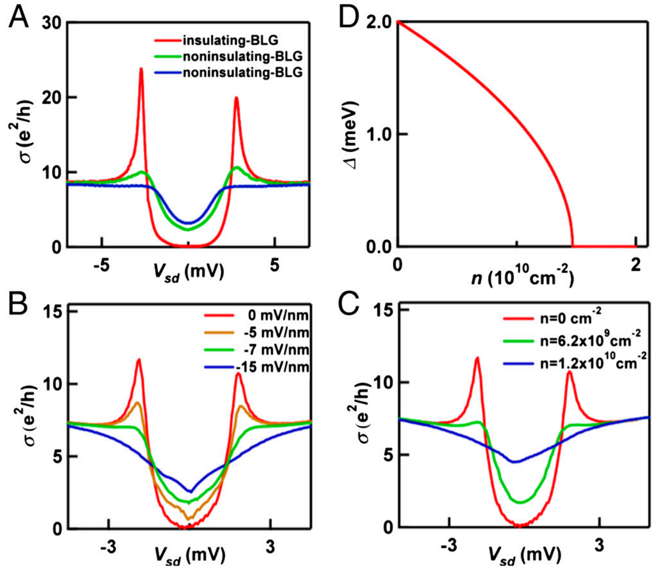

Fig. 4. (*A*) $\sigma(V_{\rm sd})$ for insulating and non-insulating BLG devices at the CNP. (*B*)$\sigma(V_{\rm sd})$ at $n = 0$ for a double-gated BLG at $E_\perp = 0$, −5, −7, and −15 mV/nm. (*C*) $\sigma(V_{\rm sd})$ at $E_\perp = 0$ for a double-gated BLG at different values of n (*D*) Magnitude of flavor gap vs. n calculated from MFT.

Discussion

Our experimental results provide strong evidence for a quantum phase transition between distinct states that is tuned by $E_\perp$, n, or charge disorder. The gapped state is susceptible to small variations in total carrier density, displacement field, and disorder, which could explain why it is not always seen in devices that appear to be of high quality. A family of gapped states in which each spin-valley flavor is spontaneously layer polarized, inducing large momentum-space Berry curvatures, has been theoretically anticipated (5, 6, 24). States within the family are distinguished by their flavor-dependent configuration of layer polarizations. In these states each flavor supports a quantized anomalous Hall conductivity contribution whose sign changes with the sense of its layer polarization. Increasing the carrier density works against order by Pauli blocking layer polarization and by increasing screening. Mean-field theory (MFT) predicts that the spontaneous quantum Hall states disappear once the carrier density is larger than 1.47×10^{10} cm^{-2}, in excellent agreement with the experimental findings in Fig. 4*D* (*SI Text*). The role of temperature in MFT (*SI Text*) is similar to that in the Bardeen-Cooper-Schrieffer theory of superconductivity and also in qualitative agreement with the experiment. Because the MFT has no Anderson's theorem to mitigate the role of disorder, gapped states are expected only in the highest-quality samples. Increasing $E_\perp$ favors configurations in which each flavor has the same layer polarization (5, 18); we presume that the large $E_\perp$ state we see has this property. Adding an external magnetic field favors configurations in which each flavor has the same sign of Hall conductivity and the carrier density at which the largest gap occurs is consequently proportional to field strength. Future work that explores the combined influence of all experimentally adjustable parameters could enable the gapped state to be uniquely assigned.

In summary, our systematic study of a large number of high-quality BLG devices suggests that ultraclean charge-neutral BLG devices undergo a phase transition at T_c of approximately 5 K from a metallic state to an insulating state with an energy gap of approximately 2–3 meV. The latter arise from electronic correlation and are likely spontaneous quantum Hall states *without* overall layer polarization (6, 22). Interestingly, increasing n or disorder has an effect that is similar to temperature on the insulating state, suggesting that these parameters can tune continuous quantum phase transitions. Increasing $E_\perp$ with either polarity will also induce a transition into a topologically different gapped state *with* layer polarization. We expect that the rich physics we have studied in BLG and the closely related phenomena that are expected in rhombohedral (ABC) stacked multilayer graphene (6, 18, 38, 41, 44) will provide considerable scope for future work.

Materials and Methods

Exfoliated BLG sheets are obtained by mechanical exfoliation and identified by color contrast in optical microscopy and Raman spectroscopy. Two different types of BLG devices are fabricated: (*i*) Graphene sheets are exfoliated on substrates or across predefined trenches that are 250 nm deep and approximately 3 μm wide, then coupled to 5-nm/50-nm Ti/Al metal electrodes through shadow mask evaporation (42). The typical back-gate coupling ratio of such devices is approximately 2.5×10^{10} $\mathrm{cm^{-2}V^{-1}}$. Because of the lithography-free fabrication process, these devices are extremely clean, with mobilities up to 450,000 $\mathrm{cm^2/(Vs)}$. (*ii*) BLG devices are fabricated with suspended top gates (43) using electron-beam lithography, and completed devices are released from the substrate by hydrofluoric-acid etching. These double-gated devices allow independent adjustment of induced charge density n and perpendicular electric field $E_\perp$. After fabrication we transfer our suspended BLG devices into a high-vacuum cryostat, and current annealing is performed at 1.5 K. Details of current-annealing procedure and the current-voltage characteristics at different stages of annealing are described in detail in *SI Text*.

ACKNOWLEDGMENTS. We thank J. Jung, S. Das Sarma, O. Vafek and Jozsef Cserti for helpful discussions. This work was supported in part by National Science Foundation CAREER DMR/0748910, NSF/1106358, NSF/0926056, ONR N00014-09-1-0724, and the Focus Center for Functional Engineered Nano Architectonics. C.N.L and M.B. acknowledge support by Defense Advanced Research Projects Agency/Defense Micro Electronics Activity H94003-10-2-1003. D.S. acknowledges support by National High Magnetic Field Laboratory UCGP 5068. A.H.M. and F.Z. were supported by Welch Foundation Grant TBF 1473 and Department of Energy DE-FG03-02ER45958. The trenches were fabricated at the University of California, Santa Barbara, CA, Nanofabrication facility. Part of this work was performed at the National High Magnetic Field Laboratory supported by NSF/DMR-0654118, the State of Florida, and the Department of Energy.

1. Novoselov KS, et al. (2006) Unconventional quantum Hall effect and Berry's phase of 2 in bilayer graphene. *Nat Phys* 2:177–180.
2. McCann E (2006) Asymmetry gap in the electronic band structure of bilayer graphene. *Phys Rev B* 74:161403.
3. Castro Neto AH, Guinea F, Peres NMR, Novoselov KS, Geim AK (2009) The electronic properties of graphene. *Rev Mod Phys* 81:109–162.
4. Min HK, Sahu B, Banerjee SK, MacDonald AH (2007) *Ab initio* theory of gate induced gaps in graphene bilayers. *Phys Rev B* 75:155115.
5. Nandkishore R, Levitov L (2010) Quantum anomalous Hall state in bilayer graphene. *Phys Rev B* 82:115124.
6. Zhang F, Jung J, Fiete GA, Niu QA, MacDonald AH (2011) Spontaneous quantum Hall states in chirally stacked few-layer graphene systems. *Phys Rev Lett* 106:156801.
7. Jung J, Zhang JF, MacDonald AH (2011) Lattice theory of pseudospin ferromagnetism in bilayer graphene: Competing interaction-induced quantum Hall states. *Phys Rev B* 83:115408.
8. Zhang F, Min H, Polini M, MacDonald AH (2010) Spontaneous inversion symmetry breaking in graphene bilayers. *Phys Rev B* 81:041402.
9. Vafek O, Yang K (2010) Many-body instability of Coulomb interacting bilayer graphene:Renormalization group approach. *Phys Rev B* 81:041401.
10. Lemonik Y, Aleiner IL, Toke C, Fal'ko VI (2010) Spontaneous symmetry breaking and Lifshitz transition in bilayer graphene. *Phys Rev B* 82:201408.
11. Castro EV, Peres NMR, Stauber T, Silva NAP (2008) Low-sensity ferromagnetism in biased bilayer graphene. *Phys Rev Lett* 100:186803.
12. Zhao Y, Cadden-Zimansky P, Jiang Z, Kim P (2010) Symmetry breaking in the zero-energy Landau level in bilayer graphene. *Phys Rev Lett* 104:066801.
13. Feldman BE, Martin J, Yacoby A (2009) Broken-symmetry states and divergent resistance in suspended bilayer graphene. *Nat Phys* 5:889–893.
14. Vafek O (2010) Interacting fermions on the honeycomb bilayer: From weak to strong coupling. *Phys Rev B* 82:205106.
15. Martin I, Blanter YM, Morpurgo AF (2008) Topological confinement in bilayer graphene. *Phys Rev Lett* 100:036804.
16. Kharitonov M (2012) Phase diagram for the $\nu = 0$ quantum Hall state in monolayer graphene Maxim Kharitonov. *Phys Rev B*, 85 p:155439.
17. Kharitonov M (2011) Correlated antiferromagnetic state in bilayer graphene., arXiv:1109.1553v1.
18. Zhang F, MacDonald AH (2012) Distinguishing spontaneous quantum Hall states in bilayer graphene. *Phys Rev Lett*, 108 p:186804.
19. Weitz RT, Allen MT, Feldman BE, Martin J, Yacoby A (2011) Broken-symmetry states and divergent resistance in suspended bilayer graphene. *Science* 330:812–816.
20. Martin J, Feldman BE, Weitz RT, Allen MT, Yacoby A (2010) Local compressibility measurements of correlated states in suspended bilayer graphene. *Phys Rev Lett* 105:256806.
21. Freitag F, Trbovic J, Weiss M, Schonenberger C (2012) Spontaneously gapped ground state in suspended bilayer graphene. *Phys Rev Lett* 108:076602.
22. Velasco J, et al. (2012) Transport spectroscopy of symmetry-broken insulating states in bilayer graphene. *Nat Nanotechnol* 7:156–160.
23. Mayorov AS, et al. (2011) Interaction-driven spectrum reconstruction in bilayer graphene. *Science* 333:860–863.
24. Min H, Borghi G, Polini M, MacDonald AH (2008) Pseudospin magnetism in graphene. *Phys Rev B* 77:041407.
25. Nandkishore R, Levitov L (2010) Flavor symmetry and competing orders in bilayer graphene., arXiv:1002.1966v1.
26. Zhu L, Aji V, Varma CM (2012) Ordered loop current states in bilayer graphene., arXiv:1202.0821v1.
27. Koshino M, Ando T (2006) Transport in bilayer graphene: Calculations within a self-consistent Born approximation. *Phys Rev B* 73:245403.
28. Katsnelson MI (2006) Minimal conductivity in bilayer graphene. *Eur Phys J B* 52:151–153.
29. Cserti J (2007) Minimal longitudinal dc conductivity of perfect bilayer graphene. *Phys Rev B* 75:033405.
30. David G, Rakya P, Oroszlany L, Cserti J (2012) Effect of the band structure topology on the minimal conductivity for bilayer graphene with symmetry breaking. *Phys Rev B*, 85 p:041402.
31. Das Sarma S, Hwang EH, Rossi E (2010) *Phys Rev B* 81:161407.
32. Das Sarma S, Hwang EH, Li Q (2011) Disorder by order in graphene., arXiv:1109.0988.
33. Trushin M, Kailasvuori J, Schliemann J, MacDonald AH (2010) Finite conductivity minimum in bilayer graphene without charge inhomogeneities. *Phys Rev B* 82:155308.
34. Tan YW, et al. (2007) Measurement of scattering rate and minimum conductivity in graphene. *Phys Rev Lett* 99:246803.
35. Adam S, Hwang EH, Galitski VM, Das Sarma S (2007) A self-consistent theory for graphene transport. *Proc Natl Acad Sci USA* 104:18392–18397.
36. Bolotin KI, Sikes KJ, Hone J, Stormer HL, Kim P (2008) Temperature-dependent transport in suspended graphene. *Phys Rev Lett* 101:096802.
37. Zhu WJ, Perebeinos V, Freitag M, Avouris P (2009) Carrier scattering, mobilities, and electrostatic potential in monolayer, bilayer, and trilayer graphene. *Phys Rev B* 80:235402.
38. Bao W, et al. (2011) Stacking-dependent band gap and quantum transport in trilayer graphene. *Nat Phys* 7:948–952.
39. Rossi E, Das Sarma S (2011) Inhomogenous electronic structure, transport gap, and percolation threshold in disordered bilayer graphene. *Phys Rev Lett* 107:155502.
40. Min H, Abergel DSL, Hwang EH, Das Sarma S (2011) Optical and transport gaps in gated bilayer graphene. *Phys Rev B* 84:041406(R).
41. Zhang F, Sahu B, Min HK, MacDonald AH (2010) Band structure of ABC-stacked graphene trilayers. *Phys Rev B* 82:035409.
42. Bao WZ, et al. (2010) Lithography-free fabrication of high quality substrate-supported and freestanding graphene devices. *Nano Res* 3:98–102.
43. Liu G, Velasco J, Bao WZ, Lau CN (2008) Fabrication of graphene *p-n-p* junctions with contactless top gates. *Appl Phys Lett* 92:203103.
44. Zhang F, Tilahun D, MacDonald AH (2012) Hund's rules for the $N = 0$ Landau levels of trilayer graphene. *Phys Rev B* 85:165139.

PHYSICS